Monthly Notices
of the
ROYAL ASTRONOMICAL SOCIETY

Mon. Not. R. Astron. Soc. **401,** 223–230 (2010) doi:10.1111/j.1365-2966.2009.15627.x

Type I X-ray bursts, burst oscillations and kHz quasi-periodic oscillations in the neutron star system IGR J17191−2821

D. Altamirano,[1⋆] M. Linares,[1] A. Patruno,[1] N. Degenaar,[1] R. Wijnands,[1] M. Klein-Wolt,[1] M. van der Klis,[1] C. Markwardt[2,3] and J. Swank[2]

[1]*Astronomical Institute, 'Anton Pannekoek', University of Amsterdam, Science Park 904, 1098XH Amsterdam, the Netherlands*
[2]*Laboratory for High-Energy Astrophysics, NASA Goddard Space Flight Center, Greenbelt, MD 20771, USA*
[3]*Department of Astronomy, University of Maryland, College Park, MD 20742, USA*

Accepted 2009 August 26. Received 2009 August 26; in original form 2009 June 15

ABSTRACT

We present a detailed study of the X-ray energy and power spectral properties of the neutron star transient IGR J17191−2821. We discovered four instances of pairs of simultaneous kilohertz quasi-periodic oscillations (kHz QPOs). The frequency difference between these kHz QPOs is between 315 and 362 Hz. We also report on the detection of five thermonuclear type I X-ray bursts and the discovery of burst oscillations at ∼294 Hz during three of them. Finally, we report on a faint and short outburst precursor, which occurred about two months before the main outburst. Our results on the broad-band spectral and variability properties allow us to firmly establish the atoll source nature of IGR J17191−2821.

Key words: accretion, accretion discs – binaries: close – stars: individual: IGR J17191−2821 – stars: individual: XTE J1747−274 – stars: neutron – X-rays: stars.

1 INTRODUCTION

Neutron star low-mass X-ray binaries (NS-LMXBs) have been extensively observed with the *Rossi X-ray Timing Explorer* (*RXTE*) during the last 13 yr. These observations have led to important discoveries, such as persistent and intermittent pulsations in accretion-powered millisecond X-ray pulsars, nearly coherent oscillations during X-ray bursts and strong quasi-periodic variability on millisecond time-scales [the so-called kilohertz quasi-periodic oscillations (kHz QPOs)].

The kHz QPOs are relatively narrow peaks in the power spectrum. They sometimes occur in pairs and are thought to reflect motion of matter around the neutron star at the inner edge of the accretion disc (see e.g. Miller, Lamb & Psaltis 1998). Up to date, kHz QPOs with similar characteristics have been detected in about 30 neutron star sources. While it is often assumed that at least one of the QPOs reflects the Keplerian motion at the inner edge of the accretion disc (see e.g. review by van der Klis 2006), models have to still satisfactorily explain the presence and characteristics of both QPOs.

Direct detection of coherent or nearly coherent pulsations is the only available method to measure the neutron star spin period in LMXBs. 10 NS-LMXBs out of more than 100 known (Liu et al. 2007) have shown coherent millisecond pulsations in their persistent emission; these systems are known as accretion-powered millisecond X-ray pulsars (AMXPs; see Wijnands 2005, for a review of the first six AMXPs discovered; for the last four see Kaaret et al. 2006; Krimm et al. 2007; Altamirano et al. 2008a; Casella et al. 2008). 16 sources to date (including the one presented in this paper) have shown nearly coherent millisecond oscillations during thermonuclear type I X-ray bursts (Watts et al. 2008, 2009). As the X-ray burst evolves, the oscillation frequency typically increases by a few Hz, approaching an asymptotic value ($\nu_{\rm BO}$) which is stable for a given source from burst to burst. This asymptotic frequency is thought to trace within a few Hz the spin frequency ($\nu_{\rm s}$) of the neutron star (Strohmayer et al. 1996). The AMXPs SAX J1808−3658 (Chakrabarty et al. 2003), XTE J1814−338 (Strohmayer et al. 2003), Aql X-1 (Casella et al. 2008) and most recently HETE J1900.1−2455 (Watts et al. 2009) have all shown that $\nu_{\rm s} \simeq \nu_{\rm BO}$, strongly supporting the idea that $\nu_{\rm BO}$ is a good tracer of $\nu_{\rm s}$.

Since the discovery of burst oscillations and two simultaneous kHz QPOs in NS-LMXBs, it was suggested that there was a relation between the neutron star spin frequency, $\nu_{\rm s}$, and the kHz QPO frequency difference $\Delta\nu = \nu_{\rm u} - \nu_{\ell}$. Although the frequency of the QPOs was found to vary ($150 \lesssim \nu_{\ell} \lesssim 900$ and $350 \lesssim \nu_{\rm u} \lesssim 1200$ Hz), initial measurements revealed that $\Delta\nu$ was consistent with being constant[1] and equal to the asymptotic burst oscillation $\nu_{\rm BO}$ (see e.g. Strohmayer et al. 1996). This was the main motivation for beat-frequency models such as the sonic-point model (Miller et al. 1998), which proposed that $\nu_{\rm u}$ reflects the Keplerian frequency at the inner edge of the disc, and that ν_{ℓ} was the beat between $\nu_{\rm u}$ and $\nu_{\rm s}$. As new observations revealed more sources showing both

⋆E-mail: d.altamirano@uva.nl

[1] At least in those sources in which $\nu_{\rm BO}$ was known. For example, $\Delta\nu$ in the NS-LMXB Sco X-1 is known to vary (see e.g. van der Klis et al. 1997).

$\nu_{\rm BO}$ and twin kHz QPOs, the relation became more complex (see Méndez & Belloni 2007; van der Klis 2008 for a detailed historical overview). As a summary, NS-LMXBs are often classified as *fast* or *slow* rotators, depending on whether the spin frequency is higher or lower than ∼400 Hz, respectively (Muno et al. 2001). It was found that generally the fast rotators follow $\Delta\nu \simeq \nu_{\rm s}/2$, while slow rotators follow $\Delta\nu \simeq \nu_{\rm s}$ (see Wijnands et al. 2003; Linares et al. 2005, and references therein). This of course implies that there is no one-to-one relation between $\Delta\nu$ and $\nu_{\rm s}$. Furthermore, it is now known that $\Delta\nu$ is not always consistent with being constant for sources with known $\nu_{\rm BO}$ (see e.g. Méndez et al. 1998; Jonker, Méndez & van der Klis 2002; Barret, Olive & Miller 2006, and references within).

The question of whether $\Delta\nu$ and $\nu_{\rm s}$ are physically related is still under debate. While current data might still be compatible with a bimodal relation, recent results suggest that this might not be the case. For example, Méndez & Belloni (2007) suggested that $\Delta\nu$ and $\nu_{\rm s}$ are unrelated and that the division between fast and slow rotators may be just an effect of the low number of sources showing both phenomena (see also Yin et al. 2007). Recently, Strohmayer, Markwardt & Kuulkers (2008) reported the discovery of burst oscillations at 414.7 Hz in the LMXB 4U 0614+091; if confirmed, these results would imply a spin frequency that is inconsistent with either $\Delta\nu \simeq \nu_{\rm s}/2$ or $\Delta\nu \simeq \nu_{\rm s}$ relations.

1.1 IGR J17191−2821

IGR J17191−2821 was discovered by the IBIS/ISGRI instrument on board *INTEGRAL* during observations of the galactic bulge monitoring (Kuulkers et al. 2007b) conducted between 2007 March 2 and 4 (Turler et al. 2007). The source was detected in the 20–40 and the 40–80 keV bands with significances of 10.4 and 4σ, and fluxes of 8.9 ± 0.9 and 5.8 ± 1.4 mCrab, respectively. The position of the source was first reported as (RA, Dec.) = (259.°77, −28.°35) (J2000) with an accuracy of 2.5 arcmin.

On 2007 March 3, *RXTE* Galactic bulge scans (Swank & Markwardt 2001) detected a source at a position consistent with that reported by Turler et al. (2007) at an intensity of 10 ± 1 mCrab in the 2–10 keV band (Swank et al. 2007). Follow-up *RXTE* observations performed 3–4 d later did not detect the source with a 3σ upper limit of 1.2 mCrab. 8 yr of Galactic bulge scans were re-analysed for contributions from a source at the position of IGR J17191−2821, but no flares brighter than 2 mCrab were found. These non-detections showed that this source is active relatively infrequently (Swank et al. 2007).

During further Galactic bulge scan observations on 2007 April 29 and May 2, IGR J17191−2821 was detected again, but at a level of 30 and 70 mCrab (2–10 keV). This suggested that the previous detection was a flare or outburst precursor. Several Astronomical Telegrams at this time communicated on the discovery of type I X-ray bursts (Klein-Wolt et al. 2007b; Markwardt et al. 2007), burst oscillations (Markwardt et al. 2007) and several episodes of kHz QPOs (Klein-Wolt et al. 2007c).

In this work, we present an intensive study of type I X-ray burst characteristics, burst oscillations and kHz QPOs of this newly discovered NS-LMXB IGR J17191−2821.

2 OBSERVATIONS AND DATA ANALYSIS

2.1 Light curves, colour diagrams and timing analysis

We use data from the *RXTE* Proportional Counter Array (PCA; for instrument information see Zhang et al. 1993; Jahoda et al. 2006). To study the long-term (days/months) L_x behaviour of the source, we used the PCA monitoring observations of the galactic bulge (Swank & Markwardt 2001). These observations are performed nine months of the year (as parts of the months of November, December, January and June are excluded due to solar constraints). The accuracy in the position of the PCA bulge scans is about 15 arcmin; the light curves are given in the ∼2–10 keV energy band.

To study the short-term (minutes or less) variability, we use PCA pointed observations. For IGR J17191−2821 there were 18 observations in one data set (92052-10) containing ∼2.5 to ∼10 ks of useful data per observation. We use the 16-s time-resolution standard 2 mode data to calculate X-ray colours. Hard and soft colours are defined as the 9.7–16.0 keV/6.0–9.7 keV and 3.5–6.0 keV/2.0–3.5 keV count rate ratio, respectively, and intensity as the 2.0–16.0 keV count rate. We removed type I X-ray bursts from the data as well as corrected by dead-time effects and for the contribution of the background. We normalized colours and intensities by those of the Crab Nebula (see Kuulkers et al. 1994; van Straaten, van der Klis & Méndez 2003, see table 2 in Altamirano et al. 2008b for average colours of the Crab Nebula per PCU).

For the Fourier timing analysis we used the event mode E_125us_64M_0_1s. Leahy normalized power spectra were constructed using data segments of 128 s and 1/8192 s time bins such that the lowest available frequency is 1/128 Hz and the Nyquist frequency 4096 Hz. No background or dead-time corrections were performed prior to the calculation of the power spectra. Unless stated explicitly, in our fits we only include those Lorentzians for which we can measure the integrated power with an accuracy of at least 3σ, based on the (negative) error in the power integrated from 0 to ∞. For the kHz QPOs, we report the centroid frequency ν_0, the full width at half-maximum (FWHM) and the rms amplitude. The quoted errors use $\Delta\chi^2 = 1.0$. The upper limits quoted in this paper correspond to a 95 per cent confidence level ($\Delta\chi^2 = 2.7$).

2.2 Energy spectra of the persistent emission

For the PCA, we used the Standard 2 data of PCU 2, which was active in all observations. The background was estimated using PCABACKEST version 6.0 (see FTOOLS). We calculated the PCU 2 response matrix for each observation using the FTOOLS routine PCARSP V10.1. For the High Energy X-ray Timing Experiment (HEXTE) instrument, spectra were accumulated for cluster B (as cluster A stopped rocking in 2006 October), excluding the damaged detector and averaging both rocking directions to measure the background spectrum. Dead-time corrections of both source and background spectra were performed using HXTDEAD V6.0. The response matrices were created using HXTRSP V3.1. Both for PCA and HEXTE, we filtered out data recorded during, and up to 30 min after passage through the South Atlantic Anomaly (SAA). We only used data when the pointing offset from the source was less than 0.°02 and the elevation of the source respect to the Earth was greater than 10°. Using XSPEC V11.3.2i (Arnaud 1996), we fitted simultaneously the PCA and HEXTE energy spectra using the 3.0–25.0 and 20.0–200.0 keV energy bands, respectively. We used a model consisting of a disc blackbody and a power law, absorbed with an equivalent hydrogen column density of $0.3 \times 10^{22}\,{\rm cm}^{-2}$ (Klein-Wolt et al. 2007a), which gave a good fit in all the observations ($\chi^2/{\rm dof} < 1.1$).

Table 1. X-ray bursts in IGR J17191−2821.

Number	Obs ID	Start time of the burst (UT, 2007)	Num. of PCUs on	Flux[a] (10^{-8} erg s^{-1} cm^{-2})	Osc. (yes/no)	Osc. rms amplitude[b] (2–17 keV)
1	92052-10-01-00	May 4 02:32:06	2	2.5 ± 0.3	Yes	6.9 ± 0.6 per cent
2	92052-10-05-00	May 7 02:39:39	2	2.9 ± 0.3	Yes	5.0 ± 1.0 per cent
3	92052-10-03-01	May 7 05:51:12	2	2.7 ± 0.3	No	<3 per cent
4	92052-10-06-00	May 8 17:08:53	3	2.6 ± 0.2	Yes	10.2 ± 1.5 per cent
5	92052-10-06-01	May 8 20:38:44	2	2.1 ± 0.3	No	<3 per cent

[a]Bolometric peak flux.
[b]Integrated amplitude of the oscillations in the 2–17 keV range.

2.3 Type I X-ray bursts

We examined the standard 1 mode data (2–60 keV, 0.125 s time resolution, no energy resolution) of the 18 observations for type I X-ray bursts; we found five episodes (see Table 1). We searched each burst for coherent pulsations using the Z_n^2 statistic (Strohmayer & Markwardt 1999). We computed Z_1^2 (i.e. assuming that the signal is sinusoidal) throughout the bursts using a sliding 2-s window with a step of 0.125 s. The Z_1^2 statistic has the same statistical properties as a Leahy normalized power spectrum, which means that for a purely random Poisson process, the powers follow a χ^2 distribution with 2 degrees of freedom (Strohmayer & Markwardt 1999). We searched the 30–4000 Hz frequency range in the 2–60 keV band and in narrower energy bands (Section 3.2).

We also created energy spectra every 0.25 s from the event mode (E_125us_64M_0_1s) data of all the PCUs that were on during the burst. Given the high count rates during the peak of the bursts, we corrected each energy spectrum for dead-time using the methods suggested by the *RXTE* team.[2] For each energy spectrum, we created the corresponding response matrix using the latest information available on the response of the instrument at the relevant times. As is common practice, we used as background the energy spectrum of the persistent emission taken seconds before each burst. (We used 100 s of the persistent emission to calculate the spectrum. However, we found no significant differences in the fits when the persistent emission before or after the burst was used, or when using data segments of different lengths between 100 and 500 s.) We used a blackbody model to fit the resulting burst spectra.[3]

[2] http://heasarc.gsfc.nasa.gov/docs/xte/recipes/pca_deadtime.html
[3] We assumed that the X-ray spectra after the persistent emission has been subtracted are Planckian and that the observed luminosity of the source is

$$L = 4\pi\sigma T^4 R^2,$$

so the unabsorbed bolometric X-ray flux may be determined using

$$F_{\rm bol} = \sigma T^4 (R/D)^2,$$

where σ is the Stefan–Boltzmann constant, T is the blackbody temperature, R the neutron star photosphere radius and D the distance to the source. The ratio $(R/D)^2$ is the normalization of the blackbody model we used (BBODYRAD – see XSPEC manual for details). We note that X-ray burst spectra are generally well described by blackbody emission, however, the emission from the neutron star and its environment (e.g. accretion disc) is expected to be more complex than simple blackbody emission (see e.g. van Paradijs 1982; London, Howard & Taam 1984; Kuulkers et al. 2003, and references therein).

3 RESULTS

3.1 Position of the source

Swift observed the source twice on 2007 March 8 (at 02:37 UT for a total of ∼800 s, and at 10:44 UT for a total of ∼1600 s – both observations were performed in PC mode). These are the only *Swift* observations performed before the bright outburst (see Section 3.4). The observations were taken in photon counting mode and did not show a source within the *INTEGRAL* error circle with an upper limit of 0.0021 counts s^{-1} (at a 95 per cent confidence level). Assuming a galactic absorption N_h of 3.4×10^{21} cm^{-2} and a photon index of 1.8, this count rate translates into an upper limit of $\sim 8.7 \times 10^{-14}$ erg s^{-1} cm^{-2} on the unabsorbed flux (approximately 0.004 mCrab in the 2–10 keV range). We found a source in the first *Swift* observation (i.e. on March 8 at 2:37 UT) located at (RA, Dec.) = (259.8114, −28.3005) (J2000, with an error of ∼9 arcsec), i.e. at a distance of about 3.5 arcmin from the position of the source as measured by *INTEGRAL*. We measured an average count rate of 0.0087 counts s^{-1}, which corresponds to an unabsorbed flux of 3.6×10^{-13} erg s^{-1} cm^{-2} or 0.02 mCrab (2–10 keV, assuming the same N_h and photon index as above). In the second *Swift* observation this source is not significantly detected (a total of three photons within a 10-pixel source error circle and zero from a background region three times as large). We place a 95 per cent confidence upper limit on the 2–10 keV unabsorbed flux of $\sim 2.0 \times 10^{-13}$ erg s^{-1} cm^{-2} (employing PIMMS[4] for an absorbed power-law spectrum with $N_h = 3.4 \times 10^{21}$ cm^{-2} and a photon index of 1.8, and applying the prescription for low number statistics given by Gehrels 1986). In Fig. 1 we show a *Swift*/XRT image during IGR J17191−2821 outburst (2007 May 10).

As noted by Klein-Wolt et al. (2007a), the formal *INTEGRAL* error circle on the position of IGR J17191−2821 would suggest that the faint source we detected with *Swift* is unrelated to IGR J17191−2821 (see Fig. 1). However, given the systematic uncertainties in the *INTEGRAL* position, both sources are probably one and the same. We note that this is not the first case in which the true position of a transient laid outside the reported *INTEGRAL*-IBIS/ISGRI error circle (see e.g. Kuulkers et al. 2007a).

3.2 Thermonuclear X-ray bursts and the distance to the source

We found five type I X-ray bursts (see Table 1). All bursts showed similar temperature, radius and bolometric flux profiles (not shown). The temperature and flux profiles were all single peaked, and reached their maxima within a second. The maximum temperature (kT) was always between 2 and 3 keV and the peak bolometric

[4] http://heasarc.gsfc.nasa.gov/Tools/w3pimms.html

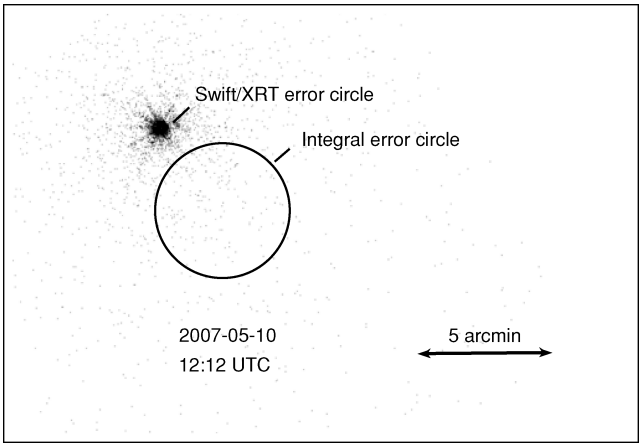

Figure 1. *Swift*/XRT image of IGR J17191−2821. The black circle represents the *INTEGRAL* error for the source position. The source showed a short (days) outburst precursor or flare on March 8. The long outburst studied in this work occurred in May (*Swift*/XRT detection is showed as bright source on the top-left of this figure).

fluxes were in the 2–3 $\times$ 10^{-8} erg s^{-1} cm^{-2} range (Table 1). In all cases, the blackbody radius remained approximately constant after the peak and was usually constrained between 5 and 10 km (assuming a distance of 11 kpc). None of the bursts showed indications of photospheric radius expansion. By using the highest measured bolometric peak flux of 3 $\times$ 10^{-8} erg s^{-1} cm^{-2} we can estimate an upper limit on the distance. We find a distance $D < 11$ kpc when using the empirically determined Eddington luminosity of 3.79 $\times$ 10^{38} erg s^{-1} (for bursts showing photospheric radius expansion; Kuulkers et al. 2003). Using a more complex approximation[5] and standard values for the mass and the radius of the neutron star (i.e. $M_{\rm NS} = 1.4\,{\rm M}_{\odot}$ and $R = 10$ km), we found $D < 8.6$ and < 6.6 for hydrogen mass fractions of $X = 0$ and 0.7, respectively. Larger values of R give higher upper limits.

3.3 kHz QPOs

We searched the averaged power spectrum of each observation for the presence of significant kHz QPOs at frequencies $\gtrsim$200 Hz. In each case, we fitted the power spectra between 200 and 4000 Hz with a model consisting of one or two Lorentzians and a constant to account for the presence of QPOs and Poisson noise, respectively. We found that 12 out of the 17 observations show significant QPOs in the 605–1185 frequency range. In four observations we detected two simultaneous kHz QPOs (see Table 2). The lower kHz QPO frequency was between 680 and 870 Hz, with single trial significance between 5.7 and 10σ. The upper kHz QPO frequency was between 1037 and 1085 Hz, with single trial significances between 3.0 and 3.7σ. $\Delta\nu$ showed no significant changes and was always consistent with 350 Hz (see Table 2).

We tried to better constrain $\Delta\nu$ by using the shift–and–add method as described by Méndez et al. (1998). We first tried to trace the detected kHz QPO using a dynamical power spectrum (e.g. see fig. 2 in Berger et al. 1996) to visualize the time evolution of the QPO frequency, but the signal was too weak to be detected on time-scales shorter than the averaged observation. Therefore, for each observation we used the fitted averaged frequency to shift each lower kHz QPO to the arbitrary frequency of 700 Hz. Next, the shifted, aligned, power spectra were averaged. The average power spectrum was finally fitted in the range 300–2048 Hz so as to exclude the edges, which are distorted due to the shifting method. To fit the averaged power spectrum, we used a function consisting of two Lorentzians and a constant to fit the QPO and the Poisson noise, respectively. In this case, the averaged $\Delta\nu$ is 332 $\pm$ 16 Hz. In Fig. 2 we show the shift-and-added power spectrum and a representative example of the single observation power spectrum with two kHz QPOs (see inset).

3.4 Outburst evolution

Fig. 3 shows the PCA light curve of IGR J17191−2821 as seen by the PCA bulge scan monitor program (Swank & Markwardt 2001). While a precursor of the outburst (see Section 1.1) occurred at MJD 54162.6, the full X-ray outburst did not start until 54 d later (i.e. MJD 54216); it lasted for about 30 d.

On MJD 54247 (2007 May 27) the source was not detected anymore with *RXTE*, and a *Chandra*/HRC-I observation was performed. As reported by Chakrabarty et al. (2007), the source was not detected in the 1.1-ks observation within the 30 arcsec of the *Swift*/XRT position (see Section 3.1). These authors estimated an upper limit on the 0.3–10 keV unabsorbed flux of $<8.3 \times 10^{-14}$ erg s^{-1} cm^{-2}.

In Fig. 4 we show the persistent unabsorbed 2–200 keV flux (panel a), power-law index (panel b), strength of the broad-band noise (panel c) and kHz QPO frequency (panel d) as a function of time during the $\sim$3 weeks of the outburst from which *RXTE* pointed observations are available. The source reached a maximum flux of $\sim$2.5 $\times$ 10^{-9} erg cm^2 s^{-1}. Assuming $D < 11$ kpc (see Section 3.2), we place an upper limit on the outburst peak luminosity of 4 $\times$ 10^{37} erg s^{-1}. In panel (a) of Fig. 4 we also plot the (type I) X-ray burst bolometric peak fluxes at the time they occurred (as detected by *RXTE*).

Because of the relatively low count rates collected by the PCA, the average power spectrum of each observation had low statistical quality. However, in the brightest (and softest) observations we found traces of the so-called very low frequency noise (VLFN). As a steep power law rising towards low frequencies, this VLFN is a typical signature of the so-called 'banana branch' (soft state) of atoll sources (see e.g. van der Klis 2006, for a review). When comparing the results showed in the different panels of Fig. 4, we found that the 5–50 Hz averaged fractional rms amplitude is anticorrelated with the source luminosity, whereas the frequencies of both kHz QPOs showed no obvious trend. The spectral index was clearly anticorrelated with the strength of the variability (i.e., correlates with luminosity). This is similar to what has been found in other atoll sources (see e.g. van der Klis 2006, for a review), where the strength of the variability and the spectral index trace the changes

[5] The approximation was recently used by Galloway et al. (2008) to compare a sample of more than a thousand X-ray burst from different sources. The distance is given by

$$D = 8.6 \left(\frac{\rm Flux_{Bol}}{3\times10^{-8}\,{\rm erg\,cm^{-2}\,s^{-1}}}\right)^{-1/2} \left(\frac{M_{\rm NS}}{1.4\,{\rm M}_{\odot}}\right)^{1/2} \times \left[\frac{1+z(R)}{1.31}\right]^{-1/2} (1+X)^{-1/2}\,{\rm kpc},$$

where $M_{\rm NS}$ is the mass of the neutron star in solar masses, X is the mass fraction of hydrogen in the neutron star atmosphere and $z(R)$ is the term that takes into account the gravitational redshift at the photosphere [where $1 + z(R) = (1 - 2GM_{\rm NS}/Rc^2)^{-1/2}$, G is the gravitational constant, c the speed of light and R the radius measured at the photosphere; see Galloway et al. 2008].

Table 2. Observations and kHz QPOs.

Obs ID (92052-10)	MJD (d)	Aver. counts/s[a] /PCU2	PCUs on[b]	Lower kHz QPO ν (Hz)	Lower kHz QPO FWHM (Hz)	Lower kHz QPO rms (per cent)	Upper kHz QPO ν (Hz)	Upper kHz QPO FWHM (Hz)	Upper kHz QPO rms (per cent)	$\Delta\nu$ (Hz)
-01-00	54224.09	182	2	–	–	–	–	–	–	–
-02-00	54225.07	170	3–4	870 ± 1	11 ± 1.7	8.5 ± 0.4	1185 ± 50	220 ± 94	9.2 ± 1.5	315 ± 50
-02-01	54225.14	188	3	866 ± 3	38 ± 6	9.2 ± 0.6	–	–	–	–
-03-00	54226.21	172	1–3	881 ± 10	132 ± 23	15 ± 1	–	–	–	–
-05-00	54227.10	142	2–3	681 ± 5	55.2 ± 15	10.3 ± 0.9	1043 ± 10	60^{+27}_{-19}	8.4 ± 1.1	362 ± 11
-03-01	54227.23	148	2	730 ± 1	13.2 ± 2.7	9.7 ± 0.6	1075 ± 12	55^{+32}_{-22}	8.5 ± 1.3	345 ± 12
-04-00	54228.01	156	3	891 ± 3	37.7 ± 7.5	9.4 ± 0.6	–	–	–	–
-04-01	54228.20	151	2–3	838 ± 1	25 ± 4	9.3 ± 0.4	–	–	–	–
-06-00	54228.70	129	2–3	946 ± 20	151^{+66}_{-41}	10.6 ± 1.2	–	–	–	–
-06-01	54228.90	130	2–3	702 ± 3	37 ± 7	10.4 ± 0.6	1037 ± 15	88^{+43}_{-27}	8.8 ± 1.1	335 ± 15
-07-00	54229.06	105	1–2	884 ± 13	108^{+53}_{-31}	15 ± 2	–	–	–	–
-07-01	54229.98	72	2	706 ± 10	83 ± 25	18 ± 2	–	–	–	–
-05-01	54230.04	70	2	682 ± 20	172^{+78}_{-55}	22.4 ± 2.8	–	–	–	–
-08-00	54231.09	46	2	–	–	–	–	–	–	–
-08-01	54231.75	27	2–3	–	–	–	–	–	–	–
-09-00	54232.01	23	3	–	–	–	–	–	–	–
-09-01	54232.08	21	3–4	–	–	–	–	–	–	–

[a]Background and dead-time corrected averaged count rate for PCU2; this PCU was on during all observations.
[b]In case the number of active PCUs changed, we report the minimum and maximum number.

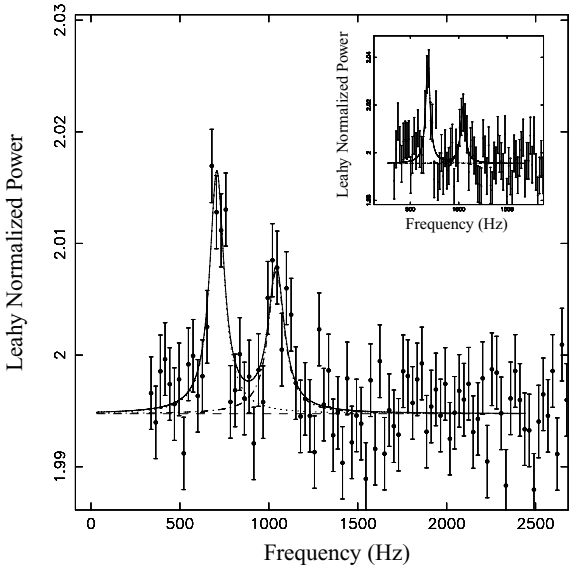

Figure 2. In the main panel we show the average kHz QPOs of all data reported in Table 2, after the shift-and-add methods was applied; the lower kHz QPO was shifted to the arbitrary frequency of 700 Hz (see Section 3.3). Inset: kHz QPOs in observation 92052-10-05-00; no shift-and-add was applied.

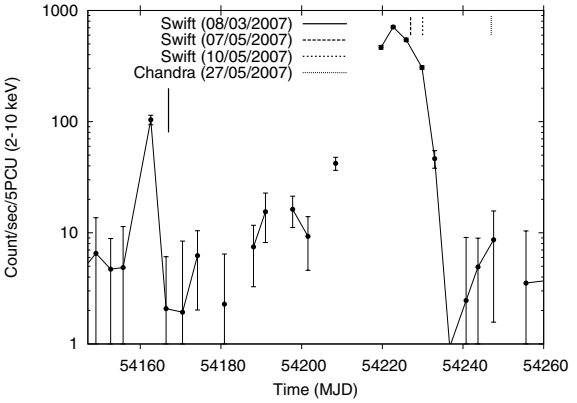

Figure 3. PCA light curve of IGR J17191−2821 as seen by the PCA bulge scan monitor program (Swank & Markwardt 2001). The times of the *Swift* and *Chandra* observations are marked with vertical lines. Contiguous non-zero measurements are connected with lines.

in the timing and spectral state during the outburst. From Fig. 4, we found that the source was initially in the soft (banana) state and showed a failed transition to the hard (extreme island) state around MJD 54226. After this, it rebrightened and returned to the soft state. On MJD 54228 (i.e. 2 d later) the luminosity reached a secondary peak and started to decline, while the source gradually transitioned from the soft (banana) state to the hard (extreme island) state. Finally IGR J17191−2821 faded below the detection limit of *RXTE*-PCA. The timing and spectral properties (and evolution) allow us to firmly establish the atoll source nature of IGR J17191−2821.

3.5 Burst oscillations

By applying the Z_1^2 method (see Section 2.3) on the 2–60 keV X-ray burst data, we discovered highly significant nearly coherent oscillations in two of the five X-ray bursts (bursts 1 and 4 in Table 1). For the remaining three bursts, we repeated the Z_1^2 analysis using only data in different energy subbands. We found that the oscillations were significantly detected also in burst number 2, but only in the 10–25 keV range. The oscillations are not significantly detected in either burst 3 or burst 5. Fractional rms amplitudes (averaged over the period the signal was significantly detected) and upper limits are given in Table 1. In Fig. 5 we show the dynamical power spectra of bursts 1 and 4 (upper and lower panels, respectively) in the 2–60 keV range. As can be seen, the frequency of the oscillations drifts from ∼291 Hz (burst 1) and ∼292.5 Hz (burst 2), to a frequency between 294 and 294.5 Hz. Maximum Z_1^2 powers of ∼63 were found in both cases. This type of frequency drifts are typical for burst oscillations during type I X-ray bursts (see e.g. Strohmayer 2001, for a review).

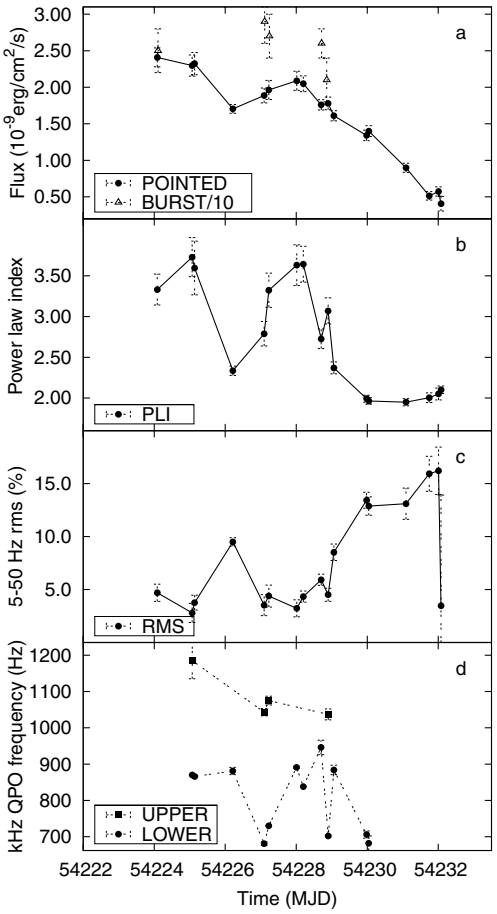

Figure 4. Spectral and timing properties along the outburst of IGR J17191−2821. From top to bottom, (a) 2–200 keV unabsorbed persistent flux (filled circles) and bolometric peak flux of the type I X-ray bursts detected by the PCA (open triangles; peak burst flux values are divided by 10 for plotting purposes); (b) power-law index obtained from the broad-band spectral fits; (c) fractional rms amplitude of the variability between 5 and 50 Hz in the ∼2.5–45 keV energy band and (d) frequencies of the upper (squares) and lower (circles) kHz QPOs detected during the outburst.

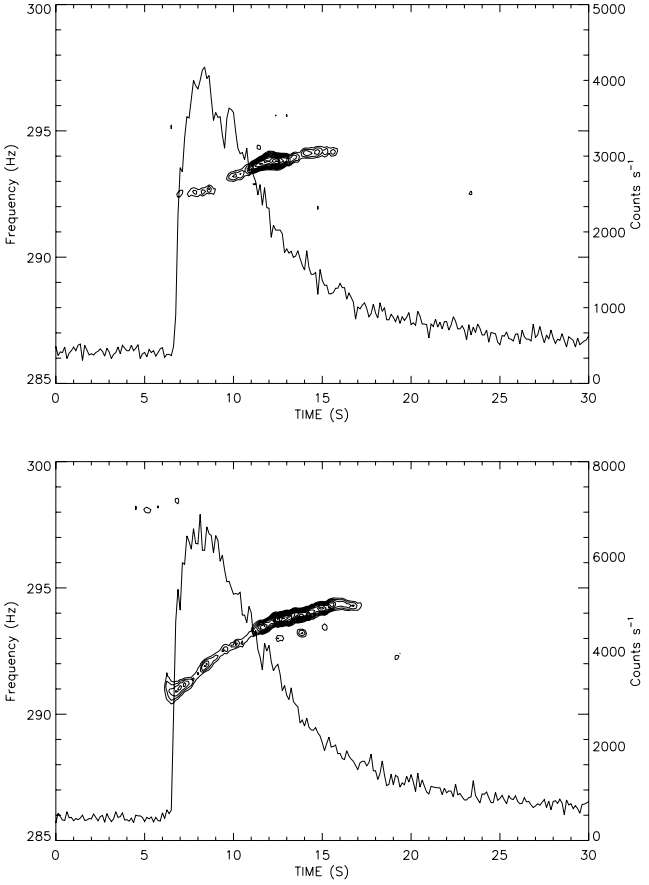

Figure 5. Light curves and dynamical power spectra (2–60 keV) for bursts 1 and 4 (upper and lower panel, respectively – see also Table 1). The dynamical power spectra were created using overlapping 2-s windows, with new windows starting at 0.125 s intervals. We used a Nyquist frequency of 4096 Hz. The contours show Leahy normalized powers between 20 and 60, increasing in steps of 5.

3.6 The energy dependence of the burst oscillations

We analysed the energy dependence of bursts 1 and 4 which showed the strongest oscillations – see Table 1. We split the data in six energy bands (from 2.5 to 17 keV), and calculated the amplitude of the pulsations in each band. To create a pulse profile in each energy band, we selected all the data with a significant pulse detection in the corresponding power spectrum, and explored the P–$\dot{P}$–$\ddot{P}$ space around a given initial guess value for the pulse period (obtained from the power spectrum). $\dot{P}$ and $\ddot{P}$ were initially set to zero. We note that $\dot{P}$ and $\ddot{P}$ do not represent true spin changes of the neutron star, but comprise all the frequency variations due, primarily, to the burst oscillation drift seen in the data. $\dot{P}$ and $\ddot{P}$ are therefore useful to align the phases of the pulsations (folded in a profile of 32 bins) for each energy band. We then fitted the pulse profiles with two sinusoids representing the fundamental and the first overtone of the burst oscillations. The errors on the fractional amplitudes are calculated using a $\Delta\chi^2 = 1$. Upper limits are at a 95 per cent confidence level (i.e. using $\Delta\chi^2 = 2.7$). We found no significant second harmonic in any of the energy bands we chose for either burst, with rms amplitude upper limits in the 2.5–17 keV range of 3.7 and 2.0 per cent, for bursts 1 and 4, respectively. The energy dependence of the burst oscillation rms amplitude is shown in Fig. 6. The fractional amplitude of the fundamental is consistent with being constant. No significant phase lags were detected.

4 DISCUSSION

We present an intensive study of the X-ray variability of the newly discovered NS-LMXB IGR J17191−2821. Our results allow us to firmly establish the atoll source nature of IGR J17191−2821. We detect several episodes of thermonuclear X-ray bursts, some of them showing burst oscillations that imply a neutron star with spin frequency of ∼294 Hz. We also detect several instances of kHz QPOs; when two were detected simultaneously, the difference in frequency is consistent with being constant (see Table 2). The energy and broadband power spectra of IGR J17191−2821 evolved in a manner consistent with that seen in other NS-LMXBs: it is soft when the flux is high and hard when the flux is low. Near the end of the outburst, IGR J17191−2821 shows the hardest spectra and strongest variability, with an rms amplitude above 15 per cent.

Two months before the main outburst, the source exhibited a very brief (only days) event which was nearly an order or magnitude less luminous. It is unclear what the relation of this event is with respect to the main outburst. However, we note that similar precursors have been seen before (see e.g. Degenaar & Wijnands 2009). To our

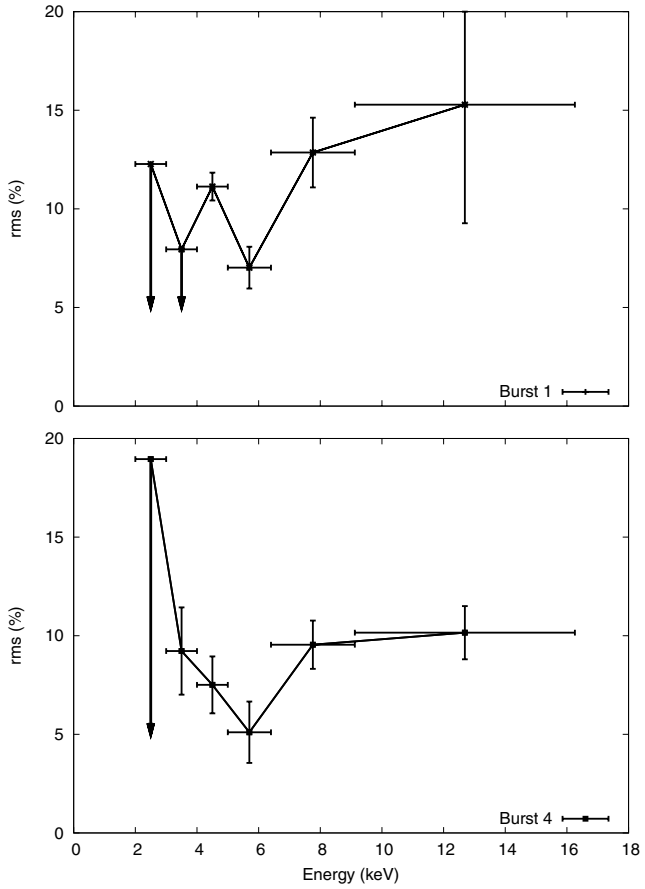

Figure 6. Fractional rms amplitude versus energy for the oscillations in X-ray bursts 1 and 4 (see Table 1). Arrows mark upper limits at 95 per cent confidence level.

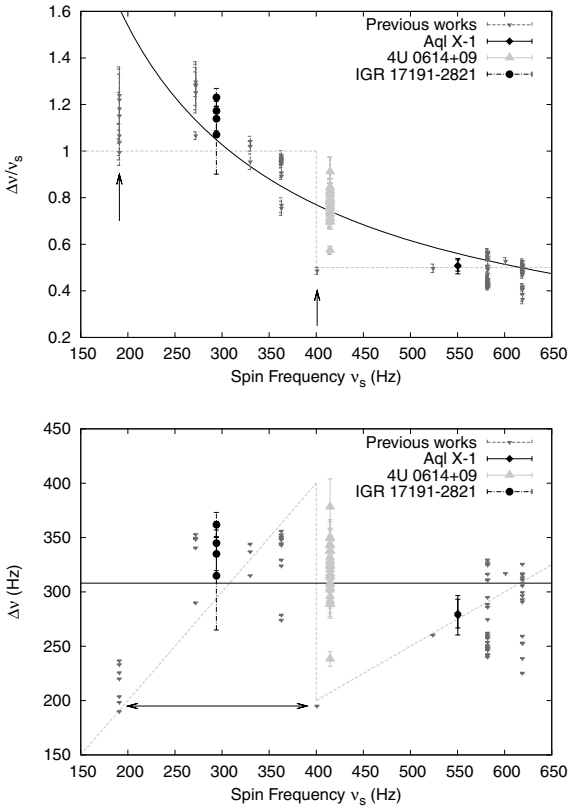

Figure 7. In the upper panel we plot the ratio between the individual measurements of $\Delta\nu = \nu_u - \nu_\ell$ and the spin frequency ν_s as a function of ν_s (cf. van der Klis 2006, 2008; Méndez & Belloni 2007). Spin frequencies are estimated from the persistent pulsations observed in AMXPs (marked with the arrows) or from burst oscillations in the non-pulsating sources. The lower panel shows the same data as above, but we plot $\Delta\nu$ versus ν_s. The dashed lines show the step function $S(\nu_s) = 1$ for $\nu_s \leq 400$ Hz; $S(\nu_s) = 0.5$ for $\nu_s > 400$ Hz. The continuous lines correspond to a constant $\Delta\nu = 308$ Hz (Méndez & Belloni 2007). For 4U 0614+09 we used the tentative burst oscillation frequency of 414.7 Hz (Strohmayer et al. 2008) and the kHz QPOs measurements reported by van Straaten et al. (2000). For Aql X-1 we used $\nu_s = 550$ Hz (e.g. Casella et al. 2008, and references within) and the tentative $\Delta\nu$ measurements reported by Barret, Boutelier & Miller (2008). IGR J17191−2821 data are from this work.

knowledge, no systematic search has been performed in order to quantify how common these precursors are and how they can be explained in the commonly used disc-instability models proposed for outbursts of X-ray binaries (see Lasota 2001, for a review).

There are currently 12 LMXBs with reported $\Delta\nu$ measurements whose spin can be estimated from either pulsations in their persistent X-ray emission or from burst oscillations (see van der Klis 2008, for a recent overview). In Fig. 7 (upper panel) we plot $\Delta\nu/\nu_s$ versus ν_s for all these sources (cf. van der Klis 2006, 2008; Méndez & Belloni 2007). The dashed line represents a step function: $\Delta\nu/\nu_s \sim 1$ for the slow rotators (<400 Hz) and $\Delta\nu/\nu_s \sim 0.5$ for the fast rotators (>400 Hz). Although most of the data seem to be consistent with this scheme (and our data of IGR J17191−2821 are as well), certainly there are points that do not follow this relation. A clear example is given by the neutron star 4U 0614+09. A tentative ∼414.7 Hz burst oscillation frequency was recently reported for this source (Strohmayer et al. 2008, note that we quote this value as tentative since it has been detected only once, the signal showed no frequency drift as expected from burst oscillations, and it was the first and only detection to date of burst oscillations with the Burst Alert Telescope on board the *Swift* telescope). As shown in Fig. 7 this burst oscillation frequency is very close to the discontinuity of the step function (although given the present data, the discontinuity of the step function could be anywhere between ∼360 and 401 Hz; furthermore, to our knowledge none of the models predicts the exact value at which $\Delta\nu/nu_s$ should switch from 1 to 0.5). At the same time, $\Delta\nu/\nu_s$ seems to cover almost the complete 0.5–1 range (van Straaten et al. 2000), although we note that 93 per cent of the $\Delta\nu/\nu_s$ measurements are in the 0.69–0.85 range and the average $\Delta\nu/\nu_s$ using all measurements is 0.767 ± 0.006 (see also Boutelier, Barret & Miller 2009).

Méndez & Belloni (2007) have recently suggested that $\Delta\nu$ and ν_s are unrelated and that the division between fast and slow rotators may be just an effect of the low number of sources showing both phenomena (see also Yin et al. 2007). In the lower panel of Fig. 7 we show $\Delta\nu$ and ν_s for the same data plotted in the upper panel. The dashed line in this panel corresponds to the average $\Delta\nu = 308$ Hz (Méndez & Belloni 2007). As can be seen, the $\Delta\nu$ range of most sources overlaps with this constant value, except for the two AMXPs SAX J1808.4−3658 and XTE J1807−294, for which $\Delta\nu$ falls clearly below 300 Hz. The discrepancy is solved, if the data for these two sources are multiplied by a factor of 1.5. This was first suggested by Méndez & Belloni (2007) based on the works of van

Straaten, van der Klis & Wijnands (2005) and Linares et al. (2005).[6] We note that not all AMXPs are affected by the same multiplicative factor (van Straaten et al. 2005), and furthermore, that the factor might be independent of whether the neutron star pulsates or not (Altamirano et al. 2005).

Clearly, the present data are not enough to draw any final conclusion on the relation between $\Delta\nu$ and ν_s; the detection of both the spin frequency and $\Delta\nu$ in other sources is necessary. The new instrument *AST ROSAT* (an Indian multiwavelength *Astronomy Satellite*), which is planned to be launched in 2010, will play a major role in solving this issue as it is likely to increase the sample of sources with both spin frequency and kHz QPOs measurements.

ACKNOWLEDGMENTS

This research has made use of data obtained from the High Energy Astrophysics Science Archive Research Center (HEASARC), provided by NASA's Goddard Space Flight Center. We are grateful to the referee for her/his comments that helped to strengthen some of the points presented in this paper.

REFERENCES

Altamirano D., van der Klis M., Méndez M., Migliari S., Jonker P. G., Tiengo A., Zhang W., 2005, ApJ, 633, 358
Altamirano D., Casella P., Patruno A., Wijnands R., van der Klis M., 2008a, ApJ, 674, L45
Altamirano D., van der Klis M., Méndez M., Jonker P. G., Klein-Wolt M., Lewin W. H. G., 2008b, ApJ, 685, 436
Arnaud K. A., 1996, in Jacoby G. H., Barnes J., eds, ASP Conf. Ser. Vol. 101, Astronomical Data Analysis Software and Systems V. Astron. Soc. Pac., San Francisco, p. 17
Barret D., Olive J. F., Miller M. C., 2006, MNRAS, 370, 1140
Barret D., Boutelier M., Miller M. C., 2008, MNRAS, 384, 1519
Berger M. et al., 1996, ApJ, 469, L13
Boutelier M., Barret D., Miller M. C., 2009, MNRAS, 399, 1901
Casella P., Altamirano D., Patruno A., Wijnands R., van der Klis M., 2008, ApJ, 674, L41
Chakrabarty D., Morgan E. H., Wijnands R., van der Klis M., Galloway D. K., Muno M. P., Markwardt C. B., 2003, BAAS, 35, 657
Chakrabarty D., Krauss M. I., Jonker P. G., Juett A. M., Markwardt C. B., 2007, Astron. Telegram, 1096, 1
Degenaar N., Wijnands R., 2009, A&A, 495, 547
Galloway D. K., Muno M. P., Hartman J. M., Psaltis D., Chakrabarty D., 2008, ApJS, 179, 360
Gehrels N., 1986, ApJ, 303, 336
Jahoda K., Markwardt C. B., Radeva Y., Rots A. H., Stark M. J., Swank J. H., Strohmayer T. E., Zhang W., 2006, ApJS, 163, 401
Jonker P. G., Méndez M., van der Klis M., 2002, MNRAS, 336, L1
Kaaret P., Morgan E. H., Vanderspek R., Tomsick J. A., 2006, ApJ, 638, 963
Klein-Wolt M., Wijnands R., Markwardt C. B., Swank J. H., 2007a, Astron. Telegram, 1025, 1
Klein-Wolt M., Wijnands R., Swank J. H., Markwardt C. B., 2007b, Astron. Telegram, 1065, 1
Klein-Wolt M., Wijnands R., Swank J. H., Markwardt C. B., 2007c, Astron. Telegram, 1075, 1
Krimm H. A. et al., 2007, ApJ, 668, L147
Kuulkers E., van der Klis M., Oosterbroek T., Asai K., Dotani T., van Paradijs J., Lewin W. H. G., 1994, A&A, 289, 795
Kuulkers E., den Hartog P. R., in't Zand J. J. M., Verbunt F. W. M., Harris W. E., Cocchi M., 2003, A&A, 399, 663
Kuulkers E. et al., 2007a, Astron. Telegram, 1008, 1
Kuulkers E. et al., 2007b, A&A, 466, 595
Lasota J. P., 2001, New Astron. Rev., 45, 449
Linares M., van der Klis M., Altamirano D., Markwardt C. B., 2005, ApJ, 634, 1250
Liu Q. Z., van Paradijs J., van den Heuvel E. P. J., 2007, A&A, 469, 807
London R. A., Howard W. M., Taam R. E., 1984, ApJ, 287, L27
Markwardt C. B., Klein-Wolt M., Swank J. H., Wijnands R., 2007, Astron. Telegram, 1068, 1
Méndez M., Belloni T., 2007, MNRAS, 381, 790
Méndez M., van der Klis M., Wijnands R., Ford E. C., van Paradijis J., Vaughan B. A., 1998, ApJ, 505, L23
Miller M. C., Lamb F. K., Psaltis D., 1998, ApJ, 508, 791
Muno M. P., Chakrabarty D., Galloway D. K., Savov P., 2001, ApJ, 553, L157
Reig P., van Straaten S., van der Klis M., 2004, ApJ, 602, 918
Strohmayer T. E., 2001, Advances Space Res., 28, 511
Strohmayer T. E., Markwardt C. B., 1999, ApJ, 516, L81
Strohmayer T. E., Zhang W., Swank J. H., Smale A., Titarchuk L., Day C., Lee U., 1996, ApJ, 469, L9
Strohmayer T. E., Markwardt C. B., Swank J. H., in't Zand J., 2003, ApJ, 596, L67
Strohmayer T. E., Markwardt C. B., Kuulkers E., 2008, ApJ, 672, L37
Swank J., Markwardt K., 2001, in Inoue H., Kunieda H., eds, ASP Conf. Ser. Vol. 251, New Century of X-ray Astronomy. Astron. Soc. Pac., San Francisco, p. 94
Swank J. H., Markwardt C. B., Klein-Wolt M., Wijnands R., 2007, Astron. Telegram, 1022, 1
Turler M. et al., 2007, Astron. Telegram, 1021, 1
van der Klis M., 2006, in Lewin W. H. G., van der Klis M., eds, Compact Stellar X-Ray Sources. Cambridge Univ. Press, Cambridge, p. 39
van der Klis M., 2008, in Wijnands R., Altamirano D., Soleri P., Degenaar N., Rea N., Casella P., Patruno A., Linares M., eds, AIP Conf. Ser. Vol. 1068. Am. Inst. Phys., New York, p. 163
van der Klis M., Wijnands R. A. D., Horne K., Chen W., 1997, ApJ, 481, L97
van Paradijs J., 1982, A&A, 107, 51
van Straaten S., Ford E. C., van der Klis M., Méndez M., Kaaret P., 2000, ApJ, 540, 1049
van Straaten S., van der Klis M., di Salvo T., Belloni T., 2002, ApJ, 568, 912
van Straaten S., van der Klis M., Méndez M., 2003, ApJ, 596, 1155
van Straaten S., van der Klis M., Wijnands R., 2005, ApJ, 619, 455
Watts A. L., Krishnan B., Bildsten L., Schutz B. F., 2008, MNRAS, 389, 839
Watts A. L. et al., 2009, ApJ, 698, L174
Wijnands R., 2005, preprint (astro-ph/0501264)
Wijnands R., van der Klis M., Homan J., Chakrabarty D., Markwardt C. B., Morgan E. H., 2003, Nat, 424, 44
Yin H. X., Zhang C. M., Zhao Y. H., Lei Y. J., Qu J. L., Song L. M., Zhang F., 2007, A&A, 471, 381
Zhang W., Giles A. B., Jahoda K., Soong Y., Swank J. H., Morgan E. H., 1993, in Siegmund O. H. W., ed., Proc. SPIE Vol. 2006, EUV, X-Ray, and Gamma-Ray Instrumentation for Astronomy IV. SPIE, Bellingham, p. 324

[6] Previous works have shown that the frequencies of the variability components observed in atoll sources follow a universal scheme of correlations when plotted versus ν_u (see e.g. van Straaten et al. 2002; van Straaten et al. 2003; Reig, van Straaten & van der Klis 2004; Altamirano et al. 2008b, and references therein). The two AMXPs SAX J1808.4−3658 and XTE J1807−294 show similar relations. However, the relations for these two sources are shifted with respect to those of the other sources (Linares et al. 2005; van Straaten et al. 2005). This shift is between the frequencies of the low-frequency components and ν_u by a factor of around 1.5 (1.45 and 1.59 for SAX J1808.4−3658 and XTE J1807−294, respectively) and between ν_ℓ and ν_u by a similar factor.

This paper has been typeset from a TEX/LATEX file prepared by the author.